Published in final edited form as:
Acta Biomater. 2014 February ; 10(2): 831–842.

Thermally responsive nanoparticle-encapsulated curcumin and its combination with mild hyperthermia for enhanced cancer cell destruction

Wei Rao[a,b], **Wujie Zhang**[f], **Izmarie Poventud-Fuentes**[g], **Yongchen Wang**[a,b], **Yifeng Lei**[a,b], **Pranay Agarwal**[a,b], **Benjamin Weekes**[a], **Chenglong Li**[d], **Xiongbin Lu**[h], **Jianhua Yu**[c,e], and **Xiaoming He**[a,b,c,*]

[a]Department of Biomedical Engineering, The Ohio State University, Columbus, OH 43210, USA

[b]Davis Heart and Lung Research Institute, The Ohio State University, Columbus, OH 43210, USA

[c]James Comprehensive Cancer Center, The Ohio State University, Columbus, OH 43210, USA

[d]Division of Medicinal Chemistry and Pharmacognosy, The Ohio State University, Columbus, OH 43210, USA

[e]Division of Hematology, The Ohio State University, Columbus, OH 43210, USA

[f]Biomolecular Engineering Program, Department of Physics and Chemistry, Milwaukee School of Engineering, Milwaukee, WI 53202, USA

[g]Department of Industrial Biotechnology, University of Puerto Rico, Mayaguez, PR 00681, USA

[h]Department of Cancer Biology, University of Texas M.D. Anderson Cancer Center, Houston, TX 77030, USA

Abstract

In this study, thermally responsive polymeric nanoparticle-encapsulated curcumin (nCCM) was prepared and characterized. The nCCM is ~22 and 300 nm in diameter at 37 and 22 °C, respectively. The smaller size of the nCCM at 37 °C was found to significantly facilitate its uptake in vitro by human prostate adenocarcinoma PC-3 cancer cells. However, the intracellular nCCM decreases rapidly (rather than plateaus) after reaching its peak at ~1.5 h during a 3-day incubation of the PC-3 cells with nCCM. Moreover, a mild hyperthermia (with negligible cytotoxicity alone) at 43 °C applied between 1 and 1.5 h during the 3-day incubation not only increases the peak uptake but also alters intracellular distribution of nCCM (facilitating its delivery into cell nuclei),

* Corresponding author at: Department of Biomedical Engineering, The Ohio State University, 1080 Carmack Road, Columbus, OH 43210, USA. Tel.: +1 614 247 8759; fax: +1 614 292 7301. he.429@osu.edu (X. He).

Disclosure

The authors declare no conflict of interests.

Appendix A. Supplementary data

Supplementary data associated with this article can be found, in the online version, at http://dx.doi.org/10.1016/j.actbio.2013.10.020.

Appendix B. Figures with essential colour discrimination

Certain figures in this article, particularly Figs. 1–7 and Scheme 1, are difficult to interpret in black and white. The full colour images can be found in the on-line version, at http://dx.doi.org/10.1016/j.actbio.2013.10.020.

which helps to retain a significantly much higher level of intracellular curcumin. These effects of mild hyperthermia could be due in part to the thermal responsiveness of the nCCM: they are more positively charged at 43 °C and can be more easily attracted to the negatively charged nuclear membrane to enter nuclei as a result of electrostatic interaction. Ultimately, a combination of the thermally responsive nCCM and mild hyperthermia significantly enhances the anticancer capability of nCCM, resulting in a more than 7-fold decrease in its inhibitory concentration to reduce cell viability to 50% (IC_{50}). Further mechanistic studies suggest injury pathways associated with heat shock proteins 27 and 70 should contribute to the enhanced cancer cell destruction by inducing cell apoptosis and necrosis. Overall, this study demonstrates the potential of combining mild hyperthermia and thermally responsive nanodrugs such as nCCM for augmented cancer therapy.

Keywords

Chitosan; Curcumin; Nanoparticle; Pluronic F127; Thermal responsiveness; Hyperthermia

1. Introduction

Curcumin, a natural compound commonly found in the food spice turmeric, has been shown to have excellent anticancer activity via various molecular and cellular pathways, and has attracted much attention for its potential use as a non-toxic anticancer agent [1–5]. As with many hydrophobic anticancer agents, however, a major hurdle to the widespread use of curcumin is its poor solubility in water and short half-life in circulation leading to poor bioavailability [6–8].

To resolve this challenge, polymeric and inorganic nanoparticles, liposomes, micelles and phospholipid complexes have been used to encapsulate curcumin for delivery with promising outcomes [9–20]. Among them, polymeric nanoparticles are emerging as one of the best options (e.g. because of their high stability compared to micelle-based delivery vehicles) [9–11]. However, polymeric nanoparticles encapsulated with curcumin (or other hydrophobic drugs in general) usually have a diameter of a few hundred nanometers, which are much bigger than the recently reported optimal size of ~10–30 nm for both cellular uptake (by endocytosis) and systemic drug delivery [21–23]. Because direct synthesis of drug-laden polymeric nanoparticles of the optimal size is difficult, we propose to use Pluronic F127 and chitosan to prepare thermally responsive nanoparticles that are ~300 nm, with a loose wall, at room temperature when encapsulating curcumin and are of the optimal size, with a tight wall, at 37 °C to withhold the curcumin for delivery. The FDA has approved Pluronic F127 (also called Poloxamer 407) as a pharmaceutical ingredient for medical use [24,25]. Chitosan, a polymer derived from chitin that is the second most abundant polysaccharide found on earth after cellulose, is non-toxic, non-inflammatory, biodegradable and positively charged [26–29]. These properties render Pluronic F127 and chitosan two of the best biopolymers for synthesizing thermally responsive multiscale vehicles to deliver therapeutic agents for medical applications, including cancer treatment [25–31]. We have previously prepared thermally responsive Pluronic F127–chitosan nanoparticles for encapsulating small hydrophilic molecules (ethidium bromide) and further

demonstrated the feasibility of utilizing the thermal responsiveness to achieve temperature-controlled release of the encapsulated small molecule [29]. However, to the best of our knowledge, no study has been reported on preparing a thermally responsive polymeric nanoparticle-encapsulated anticancer compound such as curcumin, which is hydrophobic, for cancer treatment.

On the other hand, although not effective at destroying cancer alone, mild hyperthermia (heating at supraphysiological temperatures usually below 45 °C) has been used clinically as an adjuvant treatment to effectively enhance chemo- and radiotherapy of malignant diseases for decades [32–38]. This is because mild hyperthermia can sensitize tumors to chemo- and radiotherapy by increasing the tumor blood flow and inducing an immune response against the cancer [32–38]. Recently, more severe hyperthermia with a temperature usually above 45 °C has been combined with anticancer agents either encapsulated in liposomes or conjugated on the surface of inorganic (e.g. gold, magnetic and carbon) nanoparticles to enhance cancer therapy with promising outcomes [39–50]. An additional advantage of using these inorganic nanoparticles is that, after delivered into the tumor, they can be heated in a minimally or even non-invasive way using laser or electromagnetic waves as the energy source [37,45]. However, the mechanism of hyperthermia in enhancing chemotherapy at the cellular level is still not well understood and such a combined strategy for enhanced cancer treatment, using an anticancer drug encapsulated in polymeric nanoparticles, particularly those that are thermally responsive in size and surface charge, has not been widely investigated.

In this study, we report the synthesis and characterization of thermally responsive Pluronic F127–chitosan nanoparticle-encapsulated curcumin (nCCM). The thermal responsiveness of the nCCM in both size and surface charge was found to be important for its uptake by PC-3 cancer cells. Moreover, our data demonstrate that mild hyperthermia can not only increase cellular uptake, but can also improve retention and facilitate nuclear delivery of the thermally responsive nCCM in cancer cells, which renders hyperthermia a powerful enhancer of the nCCM for cancer destruction. These results suggest that the combination of thermally responsive nCCM (and probably many other nanodrugs) and mild hyperthermia is a promising strategy for augmented cancer destruction.

2. Materials and methods

2.1. Materials

Pluronic F127 (MW: 12.6 kDa, polydispersity index or M_w/M_n~1.4 [51]) was obtained from BASF Corp (Wyandotte, MI, USA). Chitosan oligosaccharide of pharmaceutical grade (MW: 1.2 kDa, 95% deacetylation) was purchased from Zhejiang Golden-Shell Biochemical Co. Ltd (Zhejiang, China). The WST-1 cell proliferation reagent was purchased from Roche Diagnostics (Mannheim, Germany). Fetal bovine serum, penicillin and streptomycin were purchased from Hyclone (Logan, UT, USA). The F-12K cell culture medium was purchased from ATCC (Manassas, VA, USA). Curcumin (MW: 368.38 Da) from turmeric (*Curcuma longa*) with purity ≥65% was purchased from Sigma (St. Louis, MO, USA) and used without further purification. All other chemicals were purchased from Sigma unless specifically mentioned otherwise.

2.2. Synthesis of Pluronic F127–chitosan nanoparticles

The synthesis of Pluronic F127–chitosan nanoparticles in this study is a slight modification of that reported previously [29]. In short, a total of 30 ml of Pluronic F127 (see Scheme 1, *x*: 65, and *y*: 100) solution (26 mM in benzene) was added dropwise into 30 ml of 4-nitrophenyl chloroformate (4-NPC) solution (160 mM in benzene) and the mixture was stirred for 3 h in N_2 atmosphere at room temperature to activate the Pluronic F127. The activated polymer was then precipitated and filtered in excess (ice-cold) diethyl ether three times and dried under a vacuum overnight. To synthesize Pluronic F127–chitosan nanoparticles (Scheme 1), a total of 500 μl of the activated polymer (300 mg ml^{-1} or 23.2 mM) in dichloromethane was added dropwise into 5 ml of chitosan solution (15 mg ml^{-1} or 12.5 mM) in deionized (DI) water at pH 10 under sonication using a Branson 450 digital sonifier (Danbury, CT, USA) at 16% of maximum amplitude for 3 min. Dichloromethane was then removed by rotary evaporation. The resultant solution was dialyzed against DI water with a Spectra/Por dialysis tube (MWCO: 50 kDa) overnight and further dialyzed against DI water for 3 h using a 1000 kDa Spectra/Por dialysis tube with a pore size of ~100 nm. Consequently, products less than ~100 nm were removed, resulting in a yield of ~18.4% (percentage in weight of final products out of total reactants used initially). Finally, the sample was freeze-dried for 48 h to obtain dry nanoparticles.

2.3. Encapsulation of curcumin to obtain nCCM

As illustrated in Scheme 1, curcumin was encapsulated in the Pluronic F127–chitosan nanoparticles by adding 0.4 ml of curcumin solution in chloroform (2.5 mg ml^{-1}) dropwise to an aqueous solution (10 mg ml^{-1}) of Pluronic–chitosan nanoparticles in DI water under constant stirring. The volume of the nanoparticle solution was varied to obtain four different feeding ratios of curcumin to nanoparticles, as shown in Table 1. After 1 h of equilibration, the sample was transferred into a round flask to remove chloroform by rotary evaporation. All the loading steps were done at 22 °C. The sample was then filtered through a 0.45 μm filter at room temperature and lyophilized for 24 h to obtain dry nCCM, which was either used immediately or stored at −20 °C for future use. To determine the encapsulation efficiency (EE) and loading content (LC), nCCM was dispersed in ethanol (that has a similar polarity to the nanoparticle core of Pluronic F127 [52]) and the absorbance at 420 nm was measured using a Beckman Coulter (Indianapolis, IN, USA) DU800 UV–Vis spectrophotometer. The EE and LC were calculated using Eqs. (1) and (2), respectively, as follows:

$$\mathrm{EE}=(\text{weight of curcumin encapsulated in nonoparticles})/(\text{weight of curcumin fed for encapsulation}) \quad (1)$$

$$\mathrm{LC}=(\text{weight of nCCM})/(\text{weight of nCCM}+\text{weight of nanoparticle}) \quad (2)$$

2.4. Physicochemical characterization

The morphology of Pluronic F127–chitosan nanoparticles was visualized using an FEI (Hillsboro, OR, USA) Tecnai G2 transmission electron microscope (TEM), for which a carbon film-coated copper TEM grid was first glow-discharged with a Denton (Moorestown,

NJ, USA) DV-502 vacuum evaporator for ~30 s. A total of 1 μl of aqueous nanoparticle solution (4 mg ml^{-1}) was then dropped onto the grid and air-dried for ~6–7 min. The grid was then put into contact with a 12.5 μl drop of 1% (w/v) uranyl acetate solution on a Ted Pella (Redding, CA, USA) PELCO® grid holder pad. Excess solution on the grid was removed by dab drying. All procedures were performed at room temperature.

The size and surface zeta potential of nanomaterials (i.e. nanoparticles and nCCM) were assessed using a Brookhaven (Holtsville, NY, USA) 90 Plus/BI-MAS dynamic light scattering (DLS) instrument by dispersing the nanomaterials at 1 mg ml^{-1} in DI water and 1 mM aqueous KCl solution, respectively, according to the manufacturer's instructions. The resultant solutions were then filtered through 0.45 μm filter and the DLS data were obtained after equilibrating the samples at the desired temperatures for at least 30 min. Because of the core–shell structure of our nanoparticle and it being less than ~300–400 (to be shown in Section 3.1), we used the thin-shell option in the built-in software of the DLS instrument for the size measurement according to the manufacturer's instructions. For this option, the only refractive index needed by the built-in software is that of the dispersing medium (i.e. 1.331 for water in this study).

For characterization using ^1H nuclear magnetic resonance (NMR), materials were dissolved in deuterated chloroform ($CDCl_3$) or water (D_2O) and ^1H NMR spectra were obtained using a Bruker (Billerica, MA, USA) DPX 400 MHz NMR with $CDCl_3$ or D_2O as the internal reference. For Fourier transform infrared spectroscopy (FTIR) study, materials were dissolved in dichloromethane, dropped onto the FTIR sample holder and dried at room temperature to form a thin layer. The FTIR spectra were then obtained using a Perkin Elmer (Waltham, MA, USA) Spectrum 100 FTIR spectrometer. X-ray diffraction (XRD) spectra were obtained using a Scintag (Cupertino, CA, USA) XD2000 X-ray diffractometer with Cu K_α radiation ($\lambda = 0.154$ nm) at 45 kV voltage, 25 mA current, a scanning rate of 1° min^{-1} and a 2θ range from 5° to 40°.

2.5. Cell culture

Human prostate adenocarcinoma PC-3 cancer cells (ATCC, Manassas, VA, USA) were cultured in F-12K medium supplemented with 10% fetal bovine serum (FBS), 100 U ml^{-1} penicillin and 100 μg ml^{-1} streptomycin at 37 °C in a humidified 5% CO_2 incubator. The medium was changed every other day. Cells at ~70% confluence were detached for passaging and/or further experimental use.

2.6. Cellular uptake and intracellular distribution of nCCM

The intracellular curcumin taken up by cells was studied qualitatively using Zeiss (Oberkochen, Germany) Apotome (confocal-like [53,54]) structured illumination microscopy (SIM), for which type I collagen-coated glass coverslips (12 mm) were placed in 35 mm Petri dish and PC-3 cells were seeded at 1.5×10^5 cells per dish in 1 ml of medium for their attachment onto the coverslips during overnight incubation [55]. The collagen-coated glass coverslips were made by dipping the glass coverslips in type I collagen solution (1 mg ml^{-1}) in phosphate buffered saline (PBS, 1 × by default) for 1 min and then drying for 15 min in the air at room temperature before the experiments. To

investigate the effect of the size of the nCCM on its uptake, the cells were further treated with medium containing 75 nM LysoTracker Red DND-99 (to stain endo/lysosomes) and nCCM of different sizes and concentrations. After 1 h of incubation at 37 °C, the cells were washed twice with 37 °C PBS and fixed with 4% paraformaldehyde at 37 °C for 10 min. The fixed cells were then incubated with Hoechst 33342 (5 μM in PBS) for 10 min at 37 °C and washed twice with 37 °C PBS to stain their nuclei. Finally, the coverslip with attached cells was mounted onto a glass slide with anti-fade mounting medium from Vector Laboratories (Burlingame, CA, USA) for further examination. To investigate the effect of hyperthermia on the cellular uptake and intracellular distribution of ~22 nm nCCM, the cells were seeded and treated with the nCCM (10 μg ml^{-1}) and LysoTracker Red DND-99 (75 nM) for 1 h in the same way as that described above. Mild hyperthermia was then applied to the samples for 30 min, using an Echotherm (Torrey Pine Scientific, Carlsbad, CA, USA) dry bath (pre-equilibrated at 43 °C) specially designed for heating/chilling samples in cell culture plates and dishes. The cells were then washed twice with 37 °C PBS and fixed with 4% paraformaldehyde at 37 °C for 10 min either at 1.5 h (i.e. immediately after hyperthermia) or at 3 h (i.e. after further incubation at 37 °C for 1.5 h post-hyperthermia in the same medium with LysoTracker Red and nCCM). The fixed cells were further stained with Hoechst 33342 (5 μM in PBS) as mentioned above. Finally, the cells were examined using Apotome SIM. Control cells with no treatment (NT) and cells treated with free curcumin (fCCM), nanoparticles (NP) and hyperthermia alone (HT) were studied in the same way in parallel.

To quantify cellular uptake of nCCM using flow cytometry, PC-3 cells were seeded in 35 mm Petri dishes at a density of 1.5×10^5 cells per dish in 1 ml of medium and cultured overnight. The cells were then incubated with medium containing nCCM either with or without hyperthermia at 43 °C between 1 and 1.5 h. At the desired time, the cells were washed twice with 37 °C PBS, detached using trypsin/ethylenediaminetetraacetic acid (EDTA), washed again with PBS at 37 °C and finally analyzed using a BD (Franklin Lakes, NJ, USA) LSR-II flow cytometer (excited at 488 nm and detected through a 530/30 nm band pass filter) and Diva software.

2.7. Cell viability

To quantify cell viability, PC-3 cancer cells were seeded in 48-well plates at a density of 10,000 cells per well in 250 μl of medium. After overnight culture, the cells were treated with either fCCM or nCCM at various concentrations (0.1–30 μg ml^{-1}). For combined treatments, the cells were also treated with mild hyperthermia by heating using an Echotherm dry bath pre-equilibrated at 43 °C at 1–1.5, 3–3.5, 6–6.5 and 12–12.5 h to determine the opti-mal time to apply hyperthermia for the combined treatment. Control cells with no treatment and cells treated with nanoparticle alone, hyperthermia alone and the combination of nanoparticle and hyperthermia were studied in parallel. After culturing for a total of 72 h, the medium containing curcumin or nanoparticles was removed and the cells were washed twice with PBS. A total of 250 μl of fresh medium (without any curcumin or nanoparticles) and 25 μl of the Roche (Mannheim, Germany) WST-1 reagent was then added to each well. After incubating for 4 h at 37 °C, absorbance at 450 nm was measured using a Perkin Elmer (Waltham, MA, USA) VICTOR™ X4 multilabel plate reader. The total

number of viable cells in the sample was determined by interpolation using a standard curve correlating absorbance to cell density over a wide range established a priori. Cell viability was further calculated as the ratio of the cell number determined for each sample to that of control cells with no treatment.

2.8. Detection of apoptosis and necrosis

To detect apoptosis and necrosis, cells were seeded in a six-well plate at a density of 1.5×10^5 cells per well in 1 ml medium. The cell density per culture area in the six-well plate was similar to that in the 48-well plate for the above-mentioned cell viability studies. After overnight incubation, the cells were further incubated with either fCCM or nCCM (10 μg ml^{-1} in culture medium) for 48 h. For the combined treatment, a mild hyperthermia was also applied by heating the samples using an Echotherm dry bath pre-equilibrated at 43 °C from 1 to 1.5 h during the incubation. To quantify apoptosis and necrosis by flow cytometry, the cells were detached using trypsin/EDTA and collected by centrifugation at 188g for 5 min. Any remaining cells in the supernatant were further collected by centrifuging at 12,000g for 5 min. All the collected cells were then washed with cold PBS and resuspended in 100 μl of BD Pharmingen (Franklin Lakes, NJ, USA) binding buffer consisting of 0.1 M Hepes/NaOH (pH 7.4), 1.4 M NaCl and 25 mM $CaCl_2$. A total of 5 μl of allophycocyanin-conjugated annexin V and 5 μl of 7-aminoactinoactinomycin D (7-AAD, BD Pharmingen, USA) were then added and the samples analyzed using a BD (Franklin Lakes, NJ, USA) LSR-II flow cytometer. Cells treated with NT, NP, HT and NP + HT were studied in the same way in parallel.

2.9. Detection of heat shock protein expression by Western blotting

PC-3 cells were seeded in 6-well plates at 1.5×10^5 cells per well and incubated overnight. The cells were then treated with 10 μg ml^{-1} fCCM or nCCM and, for the combined treatment, the samples were also treated with mild hyperthermia by heating using an Echotherm dry bath pre-equilibrated at 43 °C from 1 to 1.5 h. After the treatments, cells were incubated at 37 °C for 48 h. They were then washed twice with 37 °C PBS, lysed using the Cell Signaling (Beverly, MA, USA) radio immunoprecipitation assay buffer supplemented with protease inhibitor (Roche, Mannheim, Germany), and incubated on ice for 30 min. The lysate was centrifuged at 12,000g for 5 min and the supernatant was collected. The total protein concentration in the lysate was determined using a Bio-Rad (Hercules, CA, USA) colorimetric protein assay reagent. A total of 5 μg of total protein from each sample was then loaded onto a 4–15% sodium dodecyl sulfate–polyacrylamide gel electrophoresis gel and further transferred to polyvinylidene difluoride (PVDF) membranes using the Bio-Rad wet transfer apparatus. The PVDF membranes were then incubated in blocking buffer (5% non-fat dry milk dissolved in 1× Tris-buffered saline with 0.1% Tween-20) for 1 h, probed with the primary antibody of heat shock proteins and glyceraldehyde 3-phosphate dehydrogenase from Cell Signaling (Beverly, MA, USA) with 1:1000 dilution using 5% bovine serum albumin dissolved in 1× Tris-buffered saline with 0.1% Tween-20 overnight at 4 °C, and further incubated with HRP (horseradish peroxidase)-conjugated secondary antibody (Cell Signaling Technology, USA, 1:2000 diluted with 5% non-fat dry milk) for 1 h at room temperature. HRP activity on the membrane was visualized on an X-ray film by immersing the membrane in Thermo

(Waltham, MA, USA) SuperSignal West Pico chemiluminescent substrate and processing with a Kodak (Rochester, NY, USA) X-ray developer.

2.10. Statistical analysis

All data are reported as the mean ± standard error of mean of results from three independent runs done at three different times. Student's two-tailed *t*-test assuming equal variance was performed using Microsoft® Excel to determine the *p* value for assessing statistical significance.

3. Results and discussion

3.1. Characterization of Pluronic F127–chitosan nanoparticles

The chemistry and procedure of Pluronic F127 activation, nanoparticle synthesis and encapsulation of curcumin in the nanoparticle are illustrated in Scheme 1. Pluronic F127 was activated (step 1) at both terminals using 4-NPC [30,31]. Successful activation was confirmed by the ^{1}H NMR spectrum of the activated polymer (Fig. 1A) showing the resonance peaks (iii and iv) at δ ~ 8.3 and 7.4 ppm that are characteristic of the aromatic protons of 4-NPC and a resonance peak (ii) at δ ~ 4.4 ppm characteristic of the terminal methylene protons in the activated Pluronic F127 [56]. These peaks are absent in the ^{1}H NMR spectrum of Pluronic F127 without activation (Fig. S1A). By integrating the areas under the resonance peak (iv) at δ ~ 7.4 ppm (for the aromatic protons of 4-NPC) and peak (i) at δ ~ 1.2 ppm (for protons in -CH_3 of Pluronic F127), 33.5 ±1.8% of terminal hydroxyl groups in Pluronic F127 are estimated to be activated by 4-NPC.

Pluronic F127–chitosan nanoparticles were prepared using an emulsification–interfacial crosslinking–solvent evaporation–dialysis method (steps 2–3–4 in Scheme 1), where the micelles of activated Pluronic F127 formed after emulsification were stabilized by crosslinking the activated polymer with chitosan on the oil–water interface via amide bond formation (see the dashed circle in the formula of crosslinked Pluronic F127–chitosan in Scheme 1). As shown in Fig. 1B, the crosslink formation was confirmed by the complete disappearance of the two characteristic peaks of 4-NPC at δ ~ 7.4 and 8.3 ppm and the simultaneous appearance of two characteristic peaks of chitosan at δ ~ 2.7 (ii, for protons in chitosan on the C2 carbon linked to the amide bond between Pluronic F127 and chitosan) and 2.0 ppm (iii, for protons in the 5% residual methyl groups of chitosan) on the ^{1}H NMR spectrum of the resultant nanoparticles [29]. By integrating the areas under the resonance peaks for both crosslinked (peak ii) and total (peak iii) chitosan and for Pluronic F127 (peak i), the total and crosslinked contents of chitosan in the nanoparticles were calculated to be 10.1 ± 0.8 and 4.0 ± 0.2 wt.%, respectively. These data suggest that ~39.6% (4.0/10.1) of the primary amine groups in chitosan are crosslinked to Pluronic F127 in the nanoparticles.

A typical TEM image of the nanoparticles (after staining using uranyl acetate) showing their core–shell morphology is given in Fig. 1C. The core is shown up as a bright/whitish area surrounded by a dark shell of crosslinked Pluronic F127–chitosan. The gray-diffused stains outside the dark shell should be residual uranyl acetate for negative staining, which was difficult to elimate and which also made it difficult to accurately determine the size our

nanoparticles using a TEM. Taking a TEM image of our core–shell hydrogel nanoparticles is actually much more challenging than taking one of a solid polymer (e.g. poly(lactic-co-glycolic acid)) or inorganic (e.g. silicon and metal) nanoparticles. Therefore, we used the TEM mainly to visualize the morphology of the nanoparticles rather than to accurately determine their size. The nanoparticles are ~300 nm at room temperature (22 °C), as determined by DLS and shown in Fig. 1D. The DLS data further show that the nanoparticles are thermally responsive in both size and surface charge (represented by surface zeta potential). The diameter is ~19 nm at 37 °C and does not change much when further heated to 43 °C. Typical size distributions of the nanoparticles at 22 and 37 °C are given in Fig. S1B. The zeta potential increases from ~9 mV at 22 °C to ~21 mV at 37 °C and to ~30 mV at 43 °C. The thermal responsiveness of the nanoparticles in size is due to the change in hydrophilic–lipophilic balance within the Pluronic F127 polymer, which leads to a decrease in nanoparticle size as a result of dehydration in the nanoparticle when the temperature increases [29]. When the nanoparticle shrinks from 22 to 37 °C, more chitosan is exposed on the nanoparticle surface (due to electrostatic expulsion between chitosan molecules), leading to a higher surface zeta potential [29]. In addition, more primary amine groups in the chitosan should be protonated (from $-NH_2$ to $-NH_3^+$) as a result of increased dissociation of water molecules (from H_2O to H^+) at higher temperature, which may explain the increase in zeta potential from 37 to 43 °C even though the nanoparticle size does not change much.

3.2. Characterization of nCCM

By utilizing the high hydrophobic affinity between curcumin and the polypropylene oxide (PPO) blocks (see Scheme 1) of Pluronic F127 on the luminal (or core) side of the nanoparticles, nCCM was obtained by mixing free curcumin (in chloroform) and nanoparticles (in water) at four different feeding ratios of curcumin to nanoparticles (1:60, 1:40, 1:30 and 1:20) in weight (see steps 5–7 in Scheme 1). Successful encapsulation is first evidenced by the much-enhanced solubility of nCCM in DI water compared to fCCM. As shown in Fig. S1C, fCCM formed visible aggregates in water and easily stuck to the hydrophobic plastic wall of the microcentrifuge tube as a result of hydrophobic interactions. In contrast, both the aqueous solution of nCCM (1:20 feeding ratio) and the wall of the centrifuge tube holding the solution were clear, indicating successful encapsulation of curcumin inside the nanoparticles to increase the water solubility of the hydrophobic anticancer compound.

The ^1H NMR spectrum (with $CDCl_3$ as the solvent) of nCCM obtained at a 1:20 feeding ratio is shown in Fig. 2A. Characteristic peaks (i–vi) of curcumin (see Fig. S1D for the ^1H NMR spectrum of fCCM) are clearly seen at $\delta \sim 5.5–8$ ppm. Interestingly, if D_2O is used as the solvent to dissolve the nCCM, the characteristic peaks of curcumin are barely observable (Fig. S1E), even though nCCM is clearly seen to be dissolved in D_2O with a homogeneous brownish appearance (Fig. S1F; the nanoparticle solution is clear). The fact that the nCCM and aggregated fCCM in D_2O have a similar brownish appearance suggests that the former was dominantly entrapped/encapsulated in the nanoparticles rather than dissolved directly in the D_2O so that it is not detectable with ^1H NMR (Fig. S1E). In contrast, both nCCM and fCCM could dissolve in $CDCl_3$, giving the same homogeneous yellowish appearance (Fig.

S1F), suggesting that nCCM is released from the nanoparticles and directly dissolved in $CDCl_3$ so that it is detectable by ^1H NMR (Fig. 2A).

The FTIR spectra of fCCM, NP, fCCM + NP and nCCM over 1400–1700 cm^{-1} are presented in Fig. 2B (the spectra over a wider range of wavenumber are presented in Fig. S1G). The peaks at ~1625 and 1515 cm^{-1} in the fCCM, fCCM + NP and nCCM are due to stretching aliphatic and aromatic C=C bonds in curcumin, respectively [57]. These data indicate the successful encapsulation of curcumin in the nanoparticles and the resultant nCCM retains the characteristic chemical structures of fCCM. On the other hand, the physical state of nCCM is different from that of fCCM because the peaks due to of X-ray diffraction (XRD) by the crystalline structure [57] of fCCM are missing in all the XRD spectra of nCCM (Fig. 2C). In other words, the nCCM encapsulated in nanoparticles should be in an amorphous rather than a crystalline state.

The EE and LC at the four feeding ratios were further quantified using UV–Vis spectrophotometry and the results are shown in Table 1. The former increases with the increase in nanoparticles for encapsulation. In contrast, the LC decreases with the increase in nanoparticles for encapsulation.

The thermal responsiveness in size and surface zeta potential of nCCM obtained at the four feeding ratios is shown in Fig. 2D and Table 1. Interestingly, the nCCM obtained at low feeding ratios (1:60 and 1:40) with a low loading content could retain the thermal responsiveness of empty Pluronic F127–chitosan nanoparticles with only a slight decrease in surface zeta potential. Typical DLS data of the size distribution of the nCCM at 22 and 37 °C are shown in Fig. S1H. On the other hand, nCCM obtained at 1:20 and 1:30 feeding ratios with a high loading content lost thermal responsiveness in size with minimal thermal responsiveness in surface charge. This is probably due to the increased curcumin (in the core and PPO layer) that interacts strongly with each other and with the PPO shell, which dominates the temperature variation-induced change in hydrophobicity of the PPO block in Pluronic F127, the driving force for shrinking of the Pluronic F127–chitosan nanoparticles in response to heating. Consequently, the nanoparticles, after encapsulating a high curcumin content (1:20 and 1:30 feeding ratios), lose their thermal responsiveness and, if the LC is too high (for the 1:20 ratio), they even shrink to a smaller size (~180 nm) than that (~300 nm) of empty nanoparticles at room temperature.

3.3. Uptake and intracellular distribution of nCCM: effect of size and mild hyperthermia

The size of nanodrugs reported in the literature varies widely from <10 nm to more than a few hundred nanometers, and few studies have been conducted to identify the optimal size of nanodrugs for cellular uptake and systemic delivery [21–23]. To understand how the size of the nCCM obtained in this study affects its cellular uptake, both the thermally responsive nCCM obtained at a 1:60 feeding ratio with a diameter of ~22 nm at 37 °C and that obtained at a 1:20 feeding ratio with a diameter of ~188 nm were incubated with PC-3 cancer cells for 1 h at 37 °C and the intracellular curcumin was studied qualitatively using Apotome SIM (confocal-like [53,54]) and quantitatively using flow cytometry. The results are shown in Fig. 3. Clearly, the cellular uptake of the ~22 nm nCCM (Fig. 3A) was much faster than that of ~188 nm nCCM (Fig. 3B) to the same nCCM concentration (10 μg ml^{-1}). Moreover, this

observation holds true even when the concentration of the ~188 nm nCCM is doubled to 20 μg ml^{-1} (Fig. 3C). Furthermore, it appears to be particularly difficult for the larger nCCM to enter the cell nuclei. The difference in uptake of the ~22 vs. 188 nm nCCM by the PC-3 cells observed from microscopy was further confirmed quantitatively by flow cytometry data to be significant (under the same concentration, 10 μg ml^{-1}; Fig. 3D and E). These results are consistent with a few recent studies that suggest a diameter of 10–30 nm is optimal for both cellular uptake and systemic delivery [21–23]. Nevertheless, it is noteworthy that, in addition to its smaller size, the more highly positive surface charge of the ~22 nm nCCM at 37 °C (see Fig. 2D) should also facilitate its uptake by mammalian cells (whose plasma membrane is usually negatively charged) as a result of electrostatic attraction [28,29,58,59]. Also of note, the high co-location of nCCM (green) and endo/lysosome stains (red) of LysoTracker Red in Fig. 3A–C suggests that endocytosis is the main mechanism of cellular uptake of nCCM. In addition, the fact that doubling the nCCM (~188 nm) concentration did not result in a doubling in intensity of curcumin in the cells (Fig. 3E) suggests that the cellular uptake of nCCM does not change linearly with nCCM concentration in the cell culture medium. This is probably because it is the slower internalization of the ~188 nCCM by the cells, rather than the nCCM concentration in the culture medium, that is the rate limiting factor determining the cellular uptake of the nCCM.

Cellular uptake of the ~22 nm nCCM (this nCCM was used by default hereafter unless it is specifically mentioned to be otherwise) at 37 °C over a 3-day incubation with PC-3 cells was further quantified using flow cytometry and the results are shown in Fig. 4. Interestingly, rather than becoming plateaued, the mean intracellular curcumin intensity decreased precipitously by ~40% at 3 h after rapidly reaching its maximum at 1.5 h. The decrease continued over 1 day, after which the intracellular curcumin plateaued at ~35% of the peak value during the following 2 days. The reason for the observed decrease is unclear and warrants further study, although one might speculate that the cells could develop some mechanism to pump out nCCM as some non-desired foreign invasion. Even more interestingly, it was found that a mild hyperthermia at 43 °C applied between 1 and 1.5 h during the 3-day incubation not only further increased the peak intracellular nCCM intensity but also eliminated the precipitous decreasing phase after reaching the peak, although cellular uptake of the nCCM during (i.e. from 1 to 1.5 h) hyperthermia treatment was slower compared to that without hyperthermia and the peak uptake was delayed to 3 h. As a result, the intracellular curcumin could be maintained at a significantly much higher level in cells with hyperthermia until day 3, when the difference became insignificant.

To unravel the possible mechanism of the effect of mild hyperthermia on cellular uptake and retention of nCCM, further studies were performed using Apotome SIM to visualize the intracellular nCCM together with the cell nuclei and endo/lysosomes under various conditions, with or without hyperthermia (Fig. 5). Green fluorescence of curcumin is not observable in cells treated with NT, HT, NP or NP + HT, as shown in Fig. S2. Cellular uptake of fCCM after 1.5 h incubation with PC-3 cancer cells at 37 °C is also negligible (Fig. 5A), presumably due to its poor aqueous solubility and bioavailability [8]. Mild hyperthermia induced a slight increase in cellular uptake of fCCM (Fig. 5B), which is consistent with the flow cytometry data shown in Fig. S3 on the cellular uptake of fCCM. This slight increase is probably due to the increase in solubility of curcumin in aqueous

solution at higher temperature and hyperthermia-induced hyperpermeability of the cell plasma membrane [37,60,61]. The latter is also probably responsible for the slower (although not significantly) uptake of nCCM during hyperthermia between 1 and 1.5 h compared to that without hyperthermia (Fig. 4) because some intracellular nCCM could diffuse out of the cells along the gradient of nCCM concentration (i.e. it is higher intracellularly after 1 h incubation at 37 °C) if the plasma membrane is hyperpermeable enough. Moreover, the further increase in intracellular curcumin to the peak value from 1.5 to 3 h in cells with hyperthermia indicates that the mild hyperthermia-induced hyperpermeability of the cell plasma membrane is reversible under the conditions of this study.

As shown in Fig. 5C, encapsulation of curcumin in the Pluronic F127–chitosan nanoparticles greatly enhances the cellular uptake of the hydrophobic small molecules into PC-3 cancer cells. This presumably is a result of the much-increased solubility of nCCM, its small size, and the high affinity between the nCCM surface and the cell plasma membrane, which facilitates the cellular uptake of nCCM by endocytosis. The latter is because chitosan is positively charged (and is thus readily attracted to the negatively charged plasma membrane of cells by electrostatic interaction) and its chemical structure resembles that of biopolymers (such as hyaluronan) in native extracellular matrix, the receptors of which are expressed in many mammalian cells [29,62,63]. The yellowish appearance in the cell cytosol of the merged micrograph in Fig. 5C indicates the large overlap between the green stain of the nCCM and the red stain of the endo/lysosomes, which again suggests that endocytosis is the main mechanism for the uptake of nCCM by PC-3 cells.

It is clearly noticeable in Fig. 5C that much less nCCM appears in the cell nuclei compared to in the cytosol. Interestingly, this heterogeneity in intracellular nCCM distribution is eliminated by mild hyperthermia, as shown in Fig. 5D. In other words, the mild hyperthermia can facilitate delivery of nCCM into the nuclei of cancer cells, which could be due at least in part to the increased surface charge (represented by the zeta potential) of the nCCM at 43 °C (see Fig. 2D) and might improve the retention of nCCM in cells, as observed in Fig. 4. Indeed, the intracellular curcumin remains at a high level and is distributed homogeneously at 3 h with hyperthermia treatment for 1–1.5 h (Fig. 5E), while it is decreased at 3 h in cells without hyperthermia (Fig. 5F). Interestingly, the distribution of nCCM in cells without hyperthermia also becomes more homogeneous at 3 h (Fig. 5F), which may explain why the rate of decrease in intracellular nCCM in the cells without hyperthermia slows down after 3 h (Fig. 4). Lastly, it is also noticeable from the differential interference contrast (DIC) images that the cells appear rounded after mild hyperthermia. However, they return to the same morphology as the cells without any treatment 1 day after the hyperthermia treatment, and the cell proliferation and viability do not seem to be affected either (Figs. S4 and 6A).

3.4. Significantly augmented cancer destruction by combining nCCM and hyperthermia

In view of the interesting observations of the cellular uptake and intracellular distribution of nCCM, we further investigated the cytotoxic effect of nCCM (in the complete cell culture medium containing 10% FBS given in Section 2.5) on PC-3 cancer cells both with and

without hyperthermia, and the results are shown in Fig. 6. First of all, HT, NP and NP + HT show negligible toxicity to PC-3 cancer cells (Fig. 6A). Clearly, treatment with nCCM alone (No HT in Fig. 6B) shows significant cytotoxicity when its concentration is higher than ~3 μg ml^{-1}. In contrast to nCCM, fCCM alone shows no obvious cytotoxicity to PC-3 cells at concentrations up to 30 μg ml^{-1} (No HT in Fig. 6C), which is not surprising in view of its poor bioavailability to cancer cells as a result of its low solubility in cell culture medium (Fig. 5A). When combined with hyperthermia, nCCM shows much higher toxicity to PC-3 cancer cells, which can be attributed in part to the better cellular uptake, nuclear delivery and retention of nCCM in the cells with hyperthermia, as shown in Figs. 4 and 5. The combination of fCCM and hyperthermia also shows higher cytotoxicity compared to fCCM alone, although the combination is still not as effective at destroying the cancer cells as nCCM alone.

Since the kinetics of nCCM uptake shown in Fig. 4 is very dynamic during the first 12 h, we further performed hyperthermia for 3–3.5, 6–6.5 and 12–12.5 h, in addition to 1–1.5 h, during the incubation of PC-3 cancer cells with fCCM and nCCM to see how the timing of the hyperthermia would impact the cytotoxicity of the combined treatment. The results for hyperthermia applied from 1 to 1.5 h are given in Fig. 6B (for nCCM) and C (for fCCM), with those for the other time intervals being given in Fig. S5. To compare the effectiveness of the combined treatment with hyperthermia applied at different times, we further quantified the IC_{50} (inhibitory concentration to reduce cell viability to 50%) by interpolation using the viability data except that for fCCM without hyperthermia and that shown in Fig. S5B for fCCM with hyperthermia. For the latter, a slight linear extrapolation up to ~40 μg ml^{-1} beyond the maximum concentration tested (30 μg ml^{-1}) was done to obtain the IC_{50}. The results are shown in Fig. 6D. For fCCM without hyperthermia, the IC_{50} is easily estimated be more than 100 μg ml^{-1}, and hyperthermia greatly reduces it to ~30 μg ml^{-1} regardless of the timing of application.

The IC_{50} for nCCM treatment alone is 7.3 ± 0.4 μg ml^{-1}, which is ~4 times lower than that of fCCM combined with hyperthermia. This value is similar to what has been reported in the literature for curcumin delivered using other carriers, such as polymeric micelles and dimethylsulfoxide [9,64]. Moreover, the combination with hyperthermia applied at all the different times could further significantly decrease the IC_{50} of nCCM, with the lowest value being 1.0 ± 0.2 μg ml^{-1} for hyperthermia applied from 1 to 1.5 h. This lowest IC_{50} of nCCM for the combined treatment is not significantly different from that for hyperthermia applied from 3 to 3.5 h ($p = 0.66$), and is more (but still not significantly) different from that for hyperthermia applied from 6 to 6.5 h ($p = 0.14$) and from 12 to 12.5 h ($p = 0.08$). Therefore, the best time to apply hyperthermia is probably at 1–3 h after nCCM treatment, which is possibly because the intracellular nCCM content is at its highest during this time window, as shown in Fig. 4, and hyperthermia can facilitate the delivery of nCCM into the cell nuclei at an earlier time to kill the cells. The latter is important because curcumin could inhibit cancer cell proliferation via direct interaction with genetic materials in cell nuclei [65]. These results should provide a useful starting point for optimizing the best timing of applying hyperthermia for future in vivo studies of the combined treatment. Here, further studies were performed to understand the mechanisms of the combined therapy of nCCM and

hyperthermia (applied from 1 to 1.5 h during incubation of cells and nCCM) in destroying cancer cells, as discussed below.

3.5. Mechanisms of injury induced by nCCM and hyperthermia

To understand the injury mechanism, cell apoptosis was studied by quantifying annexin V (labeled with fluorescence probe) binding to phosphatidylserine on the outer layer of the plasma membrane of apoptotic but not healthy cells [66]. Moreover, cell necrosis was assessed simultaneously by the presence of intracellular 7-AAD, a small cationic molecule that can penetrate into cells that are necrotic or in the late stage of apoptosis but is excluded by viable cells [67]. The quantitative flow cytometry data of cell apoptosis and necrosis are shown in Fig. 7A and B. As with NT cells, apoptosis and necrosis are negligible in cells treated with HT, NP and NP + HT, indicating the superb biocompatibility of the nanoparticles and the mildness to cells of the hyperthermia treatment in this study. In contrast, both apoptosis and necrosis are significantly higher in cells treated with nCCM + HT compared to nCCM alone, fCCM + HT and fCCM alone. In addition, many of the cells appear to become necrotic (Q1 in Fig. 7A) without first going through apoptosis (Q2 and Q3 in Fig. 7A) with the combined treatment of nCCM and HT. These data indicate mild hyperthermia is indeed a powerful enhancer of nCCM in inducing cell injury.

To further understand how the mild hyperthermia (applied from 1 to 1.5 h during incubation) could augment cancer cell destruction by nCCM, the expression of four heat shock proteins (HSPs), HSP90, 70, 60 and 27, in PC-3 cancer cells was studied by Western blotting and the results are given in Fig. 7C. First of all, nanoparticles alone do not result in any appreciable change in HSP expression, which further confirms the superb biocompatibility of the nanoparticles. In addition, none of the treatments affects the expression of HSP90 and 60 much. HSP90 has been reported in the literature to be largely constant in cells even under stress conditions [68]. Since HSP60 is a mitochondrial chaperone [68], the minimal change in its expression suggests that damage to mitochondria might not be a major factor for the enhanced cancer cell destruction of combining nCCM with mild hyperthermia. Both nCCM alone and mild hyperthermia alone elevate the expression of HSP70 and 27, and the elevation is the most apparent when they are combined, which suggests that the two HSPs should play a significant role in the mechanisms responsible for the augmented cancer destruction by the combined treatment. Increased expression of HSP27 could be activated by alterations in the cell membrane [69]. Increased expression of HSP27 and 70 has been linked to damage in both the cytoplasm and the nucleus [68,70–72]. The latter suggests the importance of the enhanced nuclear delivery of nCCM by mild hyperthermia in augmenting cancer cell destruction by nCCM. Therefore, multiple cellular processes, including damage to the cell membrane and cytoplasmic (excluding mitochondrial) and nuclear proteins, might be responsible for the enhanced cancer destruction by the combined treatment of nCCM and mild hyperthermia.

4. Conclusions

We successfully synthesized thermally responsive nCCM of ~22 nm at 37 °C with a positively charged surface, both of which were found to facilitate its uptake into both the

cytosol and nuclei of PC-3 cancer cells compared to thermally irresponsive nCCM of ~188 nm. It was further found that intracellular nCCM during a 72 h incubation of the ~22 nm nCCM with PC-3 cancer cells is very much dynamic: it reaches its peak at ~1.5 h, decreases rapidly to ~60% (at 3 h) and then slowly to ~35% (at 24 h) of the peak value, and plateaus thereafter. Moreover, a mild hyperthermia (at 43 °C at 1–1.5 h during incubation) was found to facilitate delivery of the nCCM into cell nuclei and significantly improve the retention of intracellular nCCM. As a result, the combination of nCCM and mild hyperthermia can significantly augment cancer cell destruction by nCCM with a more than 7-fold reduction in IC_{50} compared to nCCM treatment alone. This enhanced cancer cell destruction could be attributed to the much improved cellular uptake, intracellular retention and nuclear delivery of nCCM, which, together with hyperthermia, activates injury pathways associated with HSP 27 and 70 to induce cell apoptosis and necrosis. In short, we demonstrate the potential of a novel combined cancer therapy of hyperthermia and thermally responsive nCCM (and possibly other nanodrugs) for augmented cancer destruction in vitro, which warrants further studies to ascertain its safety and efficacy in vivo.

Supplementary Material

Refer to Web version on PubMed Central for supplementary material.

Acknowledgments

This work was partially supported (to X.H) by an American Cancer Society (ACS) Research Scholar Grant (# 120936-RSG-11-109-01-CDD) and the SUCCESS program of the College of Medicine at The Ohio State University. Y. J. was supported by a grant (# R01CA155521) from NIH. We thank Adriano Bellotti and Kaileen Zhang for their technical help with experiments and Jenna Dumbleton for her help with proofreading the manuscript.

References

1. Rodwell C. Curcumin curries favour? Nat Rev Cancer. 2012; 12:376.
2. Luer S, Troller R, Aebi C. Antibacterial and antiinflammatory kinetics of curcumin as a potential antimucositis agent in cancer patients. Nutr Cancer. 2012; 64:975–981. [PubMed: 22973975]
3. Agrawal DK, Mishra PK. Curcumin and its analogues: potential anticancer agents. Med Res Rev. 2010; 30:818–860. [PubMed: 20027668]
4. Tang H, Murphy CJ, Zhang B, Shen Y, Van Kirk EA, Murdoch WJ, et al. Curcmin polymers as anticancer conjugates. Biomaterials. 2010; 31:7139–7149. [PubMed: 20591475]
5. Sharma RA, Euden SA, Platton SL, Cooke DN, Shafayat A, Hewitt HR, et al. Phase clinical trial of oral curcumin: biomarkers of systemic activity and compliance. Clin Cancer Res. 2004; 10:6847–6854. [PubMed: 15501961]
6. Anand P, Kunnumakkara AB, Newman RA, Aggarwal BB. Bioavailability of curcumin: problems and promises. Mol Pharm. 2007; 4:807–818. [PubMed: 17999464]
7. Garcea G, Jones DJ, Singh R, Dennison AR, Farmer PB, Sharma RA, et al. Detection of curcumin and its metabolites in hepatic tissue and portal blood of patients following oral administration. Br J Cancer. 2004; 90:1011–1015. [PubMed: 14997198]
8. Tonnesen HH, Masson M, Loftsson T. Studies of curcumin and curcuminoids. XXVII. Cyclodextrin complexation: solubility, chemical and photochemical stability. Int J Pharm. 2002; 244:127–135. [PubMed: 12204572]
9. Bisht S, Feldmann G, Soni S, Ravi R, Karikar C, Maitra A, et al. Polymeric nanoparticle-encapsulated curcumin ("nanocurcumin"): a novel strategy for human cancer therapy. J Nanobiotechnol. 2007; 5:3.

10. Chun YS, Bisht S, Chenna V, Pramanik D, Yoshida T, Hong SM, et al. Intraductal administration of a polymeric nanoparticle formulation of curcumin (NanoCurc) significantly attenuates incidence of mammary tumors in a rodent chemical carcinogenesis model: implications for breast cancer chemoprevention in at-risk populations. Carcinogenesis. 2012; 33:2242–2249. [PubMed: 22831956]
11. Lim KJ, Bisht S, Bar EE, Maitra A, Eberhart CG. A polymeric nanoparticle formulation of curcumin inhibits growth, clonogenicity and stem-like fraction in malignant brain tumors. Cancer Biol Ther. 2011; 11:464–473. [PubMed: 21193839]
12. Yallapu MM, Othman SF, Curtis ET, Gupta BK, Jaggi M, Chauhan SC. Multifunctional magnetic nanoparticles for magnetic resonance imaging and cancer therapy. Biomaterials. 2011; 32:1890–18905. [PubMed: 21167595]
13. Orr WS, Denbo JW, Saab KR, Myers AL, Ng CY, Zhou J, et al. Liposome-encapsulated curcumin suppresses neuroblastoma growth through nuclear factor-kappa B inhibition. Surgery. 2012; 151:736–744. [PubMed: 22284765]
14. Wang D, Veena MS, Stevenson K, Tang C, Ho B, Suh JD, et al. Liposome-encapsulated curcumin suppresses growth of head and neck squamous cell carcinoma in vitro and in xenografts through the inhibition of nuclear factor kappaB by an AKT-independent pathway. Clin Cancer Res. 2008; 14:6228–636. [PubMed: 18829502]
15. Leung MH, Colangelo H, Kee TW. Encapsulation of curcumin in cationic micelles suppresses alkaline hydrolysis. Langmuir. 2008; 24:5672–5675. [PubMed: 18459746]
16. Yang R, Zhang S, Kong D, Gao X, Zhao Y, Wang Z. Biodegradable polymer- curcumin conjugate micelles enhance the loading and delivery of low-potency curcumin. Pharm Res. 2012; 29:3512–3525. [PubMed: 22961588]
17. Allegri P, Mastromarino A, Neri P. Management of chronic anterior uveitis relapses: efficacy of oral phospholipidic curcumin treatment. Long-term follow-up. Clin Ophthalmol. 2010; 4:1201–1206. [PubMed: 21060672]
18. Liu A, Lou H, Zhao L, Fan P. Validated LC/MS/MS assay for curcumin and tetrahydrocurcumin in rat plasma and application to pharmacokinetic study of phospholipid complex of curcumin. J Pharm Biomed Anal. 2006; 40:720–727. [PubMed: 16316738]
19. Yallapu MM, Jaggi M, Chauhan SC. Curcumin nanoformulations: a future nanomedicine for cancer. Drug Discov Today. 2012; 17:71–80. [PubMed: 21959306]
20. Yan H, Teh C, Sreejith S, Zhu L, Kwok A, Fang W, et al. Functional mesoporous silica nanoparticles for photothermal-controlled drug delivery in vivo. Angew Chem Int Ed Engl. 2012; 51:8373–8377. [PubMed: 22777795]
21. Gao H, Shi W, Freund LB. Mechanics of receptor-mediated endocytosis. Proc Natl Acad Sci U S A. 2005; 102:9469–9474. [PubMed: 15972807]
22. Chauhan VP, Stylianopoulos T, Martin JD, Popovic Z, Chen O, Kamoun WS, et al. Normalization of tumour blood vessels improves the delivery of nanomedicines in a size-dependent manner. Nat Nanotechnol. 2012; 7:383–388. [PubMed: 22484912]
23. Cabral H, Matsumoto Y, Mizuno K, Chen Q, Murakami M, Kimura M, et al. Accumulation of sub-100 nm polymeric micelles in poorly permeable tumours depends on size. Nat Nanotechnol. 2011; 6:815–823. [PubMed: 22020122]
24. FDA. “Poloxamer 407”. U.S. Food and Drug Administration. 2013
25. Wittemann A, Azzam T, Eisenberg A. Biocompatible polymer vesicles from biamphiphilic triblock copolymers and their interaction with bovine serum albumin. Langmuir. 2007; 23:2224–2230. [PubMed: 17279718]
26. Prabaharan M. Review paper: chitosan derivatives as promising materials for controlled drug delivery. J Biomater Appl. 2008; 23:5–36. [PubMed: 18593819]
27. Riva R, Ragelle H, des Rieux A, Duhem N, Jerome C, Preat V. Chitosan and chitosan derivatives in drug delivery and tissue engineering. Adv Polym Sci. 2011; 244:19–44.
28. Yue ZG, Wei W, Lv PP, Yue H, Wang LY, Su ZG, et al. Surface charge affects cellular uptake and intracellular trafficking of chitosan-based nanoparticles. Biomacromolecules. 2011; 12:2440–2446. [PubMed: 21657799]

29. Zhang W, Gilstrap K, Wu L, K CR, Moss MA, Wang Q, et al. Synthesis and characterization of thermally responsive pluronic F127-chitosan nanocapsules for controlled release and intracellular delivery of small molecules. ACS Nano. 2010; 4:6747–6759. [PubMed: 21038924]
30. Choi SH, Lee SH, Park TG. Temperature-sensitive pluronic/poly(ethylenimine) nanocapsules for thermally triggered disruption of intracellular endosomal compartment. Biomacromolecules. 2006; 7:1864–1870. [PubMed: 16768408]
31. Zhang W, Rong J, Wang Q, He X. The encapsulation and intracellular delivery of trehalose using a thermally responsive nanocapsule. Nanotechnology. 2009; 20:275101. [PubMed: 19528681]
32. Storm, FK. Hyperthermia in cancer therapy. Boston, MA: GK Hall Medical Publisher; 1989.
33. Gautherie, M. Biological basis of oncologic thermotherapy. Berlin: Springer-Verlag; 1990.
34. Hall, EJ.; Glaccia, AJ. Hyperthermia. In: Mitchell, CW., editor. Radiobiology for the radiobiologist. 7th ed. Philadelphia, PA: Lippincott; 2011. [chapter 28]
35. Paliwal, BR.; Hetzel, FW.; Dewhirst, MW. Biological, physical and clinical aspects of hyperthermia. New York: American Institute of Physics; 1987.
36. Fıeld, B.; Hand, JW. Introduction to the clinical aspects of clinical hyperthermia. Philadelphia, PA: Taylor & Francis; 1990.
37. He X. Thermostability of biological systems: fundamentals, challenges, and quantification. Open Biomed Eng J. 2011; 5:47–73. [PubMed: 21769301]
38. He X, Bischof JC. Quantification of temperature and injury response in thermal therapy and cryosurgery. Crit Rev Biomed Eng. 2003; 31:355–422. [PubMed: 15139301]
39. Rao W, Deng Z-S, Liu J. A review of hyperthermia combined with radiotherapy/chemotherapy on malignant tumors. Crit Rev Biomed Eng. 2010; 38:101–116. [PubMed: 21175406]
40. Visaria RK, Griffin RJ, Williams BW, Ebbini ES, Paciotti GF, Song CW, et al. Enhancement of tumor thermal therapy using gold nanoparticle-assisted tumor necrosis factor-alpha delivery. Mol Cancer Ther. 2006; 5:1014–1020. [PubMed: 16648573]
41. Han HD, Choi MS, Hwang T, Song CK, Seong H, Kim TW, et al. Hyperthermia-induced antitumor activity of thermosensitive polymer modified temperature-sensitive liposomes. J Pharm Sci. 2006; 95:1909–1917. [PubMed: 16795016]
42. Kong G, Dewhirst MW. Hyperthermia and liposomes. Int J Hyperthermia. 1999; 15:345–370. [PubMed: 10519688]
43. Ponce AM, Vujaskovic Z, Yuan F, Needham D, Dewhirst MW. Hyperthermia mediated liposomal drug delivery. Int J Hyperthermia. 2006; 22:205–213. [PubMed: 16754340]
44. Dewhirst MW. Hyperthermia and nanotechnology - a note from the Editor-in-chief. Int J Hyperthermia. 2008; 24:449–450. [PubMed: 18923988]
45. Day ES, Morton JG, West JL. Nanoparticles for thermal cancer therapy. J Biomech Eng. 2009; 131:074001. [PubMed: 19640133]
46. Dennis CL, Jackson AJ, Borchers JA, Hoopes PJ, Strawbridge R, Foreman AR, et al. Nearly complete regression of tumors via collective behavior of magnetic nanoparticles in hyperthermia. Nanotechnology. 2009; 20:395103. [PubMed: 19726837]
47. Burke A, Ding X, Singh R, Kraft RA, Levi-Polyachenko N, Rylander MN, et al. Long-term survival following a single treatment of kidney tumors with multiwalled carbon nanotubes and near-infrared radiation. Proc Natl Acad Sci U S A. 2009; 106:12897–12902. [PubMed: 19620717]
48. Park H, Yang J, Lee J, Haam S, Choi IH, Yoo KH. Multifunctional nanoparticles for combined doxorubicin and photothermal treatments. ACS Nano. 2009; 3:2919–2926. [PubMed: 19772302]
49. Gilstrap K, Hu X, Lu X, He X. Nanotechnology for energy-based cancer therapies. Am J Cancer Res. 2011; 1:508–520. [PubMed: 21984969]
50. Strong LE, West JL. Thermally responsive polymer-nanoparticle composites for biomedical applications. Wiley Interdiscip Rev Nanomed Nanobiotechnol. 2011; 3:307–317. [PubMed: 21384563]
51. Jiang J, Malal R, Li C, Lin MY, Colby RH, Gersappe D, et al. Rheology of thermoreversible hydrogels from multiblock associating copolymers. Macromolecules. 2008; 41:3646–3652.
52. Croy SR, Kwon GS. The effects of pluronic block copolymers on the aggregation state of nystatin. J Control Release. 2004; 95:161–171. [PubMed: 14980765]

53. Weigel A, Schild D, Zeug A. Resolution in the ApoTome and the confocal laser scanning microscope: comparison. J Biomed Opt. 2009; 14:014022. [PubMed: 19256710]
54. Gines, TB.; Davidson, MW. Structured illumination: ZEISS ApoTome. http://zeiss-campus.magnet.fsu.edu/tutorials/opticalsectioning/apotome/index.html
55. Cain, R.; d'Água, BB.; Ridley, A. Quantification of transendothelial migration using three-dimensional confocal microscopy. In: Wells, CM.; Parsons, M., editors. Cell migration. New York: Humana Press; 2011. p. 167-90.
56. Cho K, Choi S, Park T. Low molecular weight PEI conjugated pluronic copolymer: useful additive for enhancing gene transfection efficiency. Macromol Res. 2006; 14:348–353.
57. Mohanty C, Sahoo SK. The in vitro stability and in vivo pharmacokinetics of curcumin prepared as an aqueous nanoparticulate formulation. Biomaterials. 2010; 31:6597–6611. [PubMed: 20553984]
58. Frohlich E. The role of surface charge in cellular uptake and cytotoxicity of medical nanoparticles. Int J Nanomed. 2012; 7:5577–5591.
59. Verma A, Stellacci F. Effect of surface properties on nanoparticle-cell interactions. Small. 2010; 6:12–21. [PubMed: 19844908]
60. He XM, Amin AA, Fowler A, Toner M. Thermally induced introduction of trehalose into primary rat hepatocytes. Cell Preserve Technol. 2006; 4:178–187.
61. Bhowmick S, Swanlund DJ, Bischof JC. Supraphysiological thermal injury in Dunning AT-1 prostate tumor cells. J Biomech Eng. 2000; 122:51–59. [PubMed: 10790830]
62. Jayakumar R, Menon D, Manzoor K, Nair SV, Tamura H. Biomedical applications of chitin and chitosan based nanomaterials - a short review. Carbohyd Polym. 2010; 82:227–232.
63. Hussain A, Collins G, Yip D, Cho CH. Functional 3-D cardiac co-culture model using bioactive chitosan nanofiber scaffolds. Biotechnol. Bioeng. 2013; 110:637–647. [PubMed: 22991229]
64. Yu J, Peng Y, Wu LC, Xie Z, Deng Y, Hughes T, et al. Curcumin down-regulates DNA methyltransferase 1 and plays an anti-leukemic role in acute myeloid leukemia. PLoS ONE. 2013; 8:e55934. [PubMed: 23457487]
65. Kunnumakkara AB, Anand P, Aggarwal BB. Curcumin inhibits proliferation, invasion, angiogenesis and metastasis of different cancers through interaction with multiple cell signaling proteins. Cancer Lett. 2008; 269:199–225. [PubMed: 18479807]
66. Bharti AC, Donato N, Singh S, Aggarwal BB. Curcumin (diferuloylmethane) down-regulates the constitutive activation of nuclear factor-kappa B and IkappaBalpha kinase in human multiple myeloma cells, leading to suppression of proliferation and induction of apoptosis. Blood. 2003; 101:1053–1062. [PubMed: 12393461]
67. Zimmermann M, Meyer N. Annexin V/7-AAD staining in keratinocytes. Methods Mol Biol. 2011; 740:57–63. [PubMed: 21468968]
68. Creagh EM, Sheehan D, Cotter TG. Heat shock proteins - modulators of apoptosis in tumour cells. Leukemia. 2000; 14:1161–1173. [PubMed: 10914538]
69. Martin-Ventura JL, Nicolas V, Houard X, Blanco-Colio LM, Leclercq A, Egido J, et al. Biological significance of decreased HSP27 in human atherosclerosis. Arterioscler Thromb Vasc Biol. 2006; 26:1337–1343. [PubMed: 16574891]
70. Arrigo AP, Suhan JP, Welch WJ. Dynamic changes in the structure and intracellular locale of the mammalian low-molecular-weight heat shock protein. Mol Cell Biol. 1988; 8:5059–5071. [PubMed: 3072471]
71. Pockley AG. Heat shock proteins as regulators of the immune response. Lancet. 2003; 362:469–476. [PubMed: 12927437]
72. Diller KR. Stress protein expression kinetics. Annu Rev Biomed Eng. 2006; 8:403–424. [PubMed: 16834562]

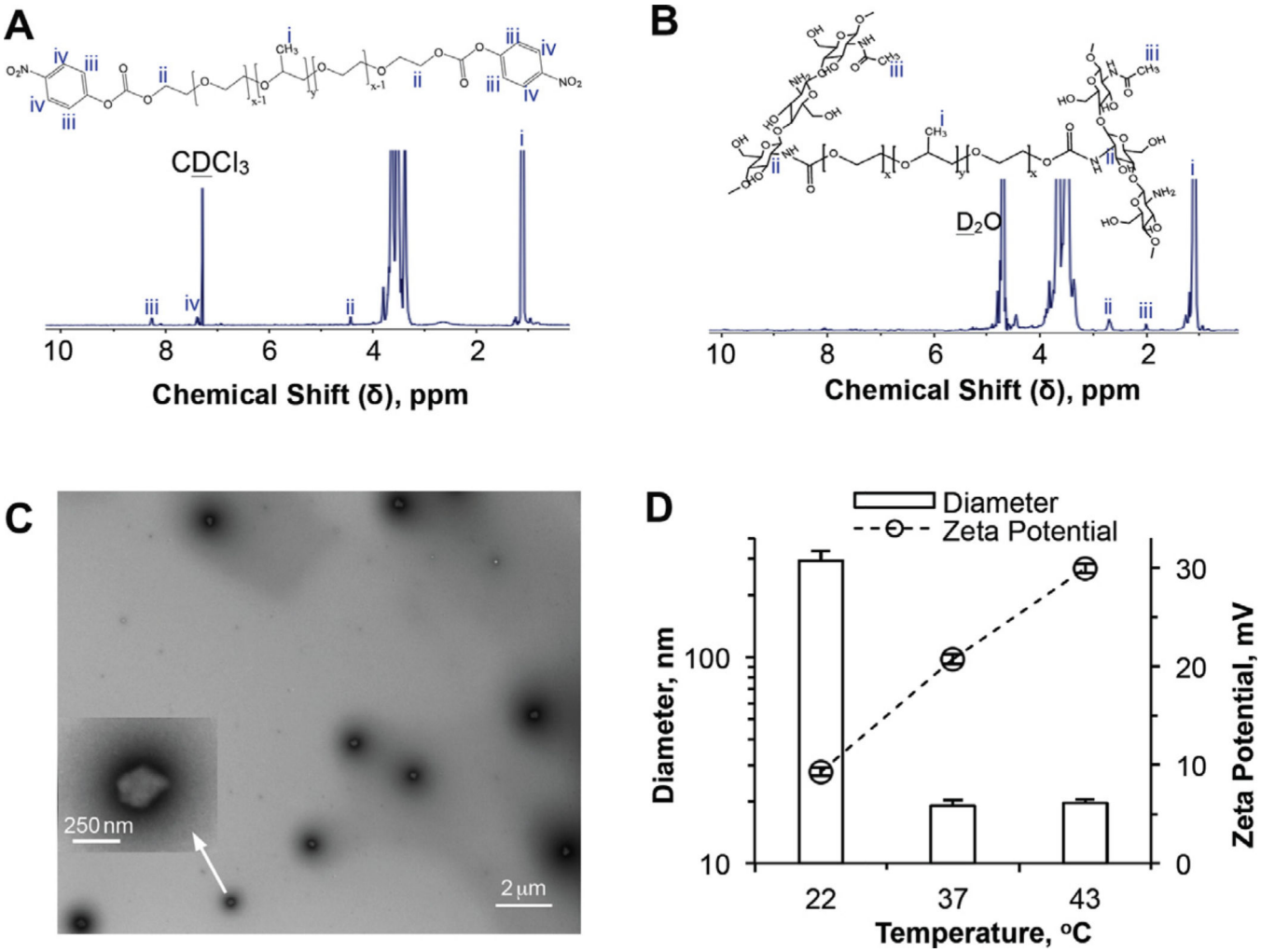

Fig. 1.

Characterization of activated Pluronic F127 and Pluronic F127–chitosan nanoparticles: ^{1}H NMR spectra of (A) 4-NPC activated Pluronic F127 in $CDCl_3$ and (B) Pluronic F127–chitosan nanoparticles in D_2O, showing characteristic peaks of 4-NPC and chitosan, respectively; (C) TEM image of Pluronic F127–chitosan nanoparticles showing their core–shell morphology (the inset shows a zoom-in view of one of the nanoparticles); and (D) DLS data showing thermal responsiveness of the nanoparticles in size (diameter) and surface charge (represented by zeta potential).

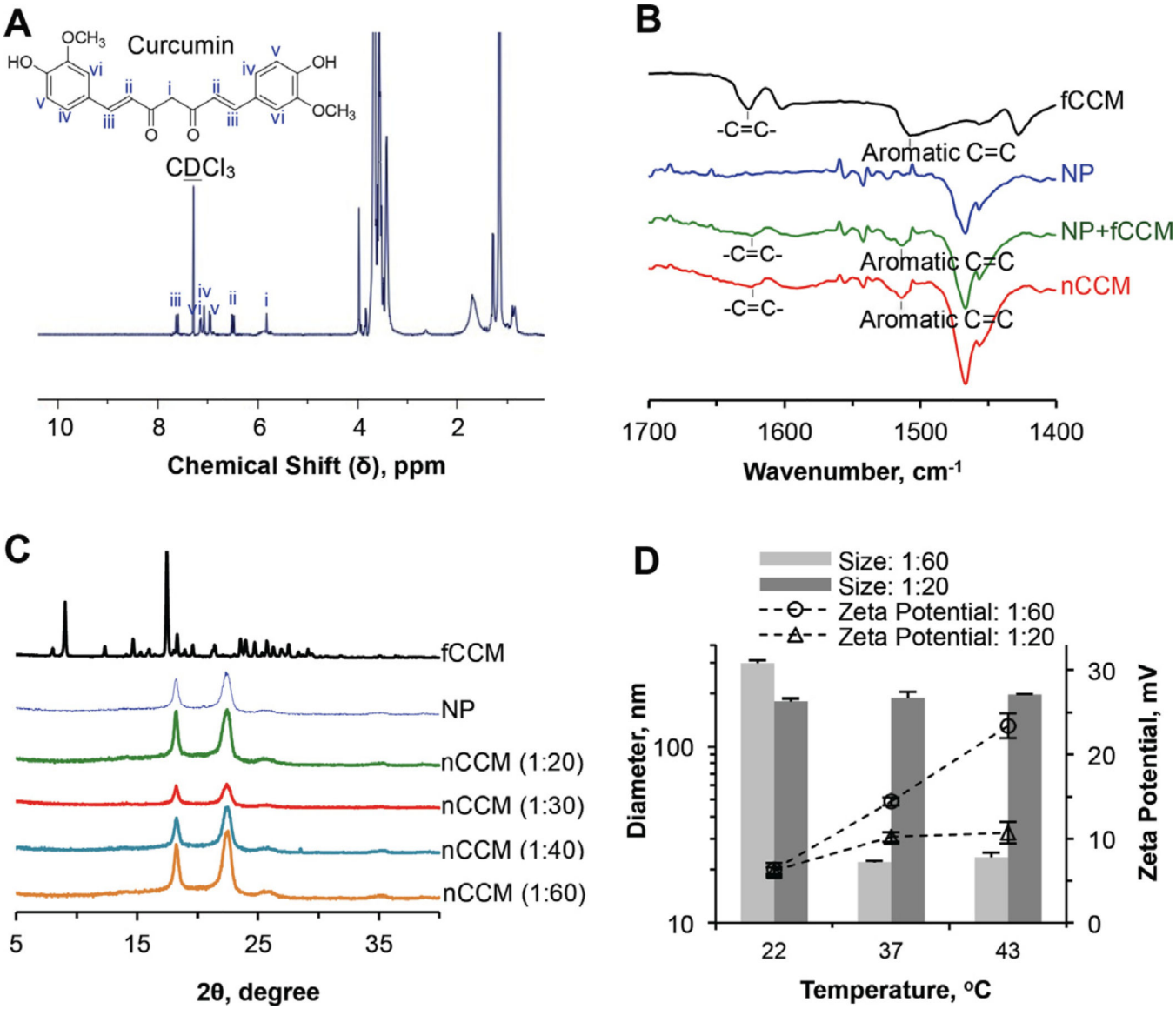

Fig. 2.

Characterization of nCCM: (A) ^{1}H NMR spectrum showing successful encapsulation of curcumin in Pluronic F127–chitosan nanoparticles to obtain nCCM; (B) FTIR spectra of fCCM, NP, a simple mixture of NP and fCCM (NP + fCCM) and nCCM, showing characteristic peaks due to the aliphatic and aromatic double bonds in curcumin; (C) XRD data showing no clear curcumin peak for nCCM obtained under different feeding ratios of curcumin to nanoparticles, indicating the amorphous state of nCCM in nanoparticles; and (D) DLS data of diameter and surface zeta potential of nCCM obtained with feeding ratios of 1:60 and 1:20.

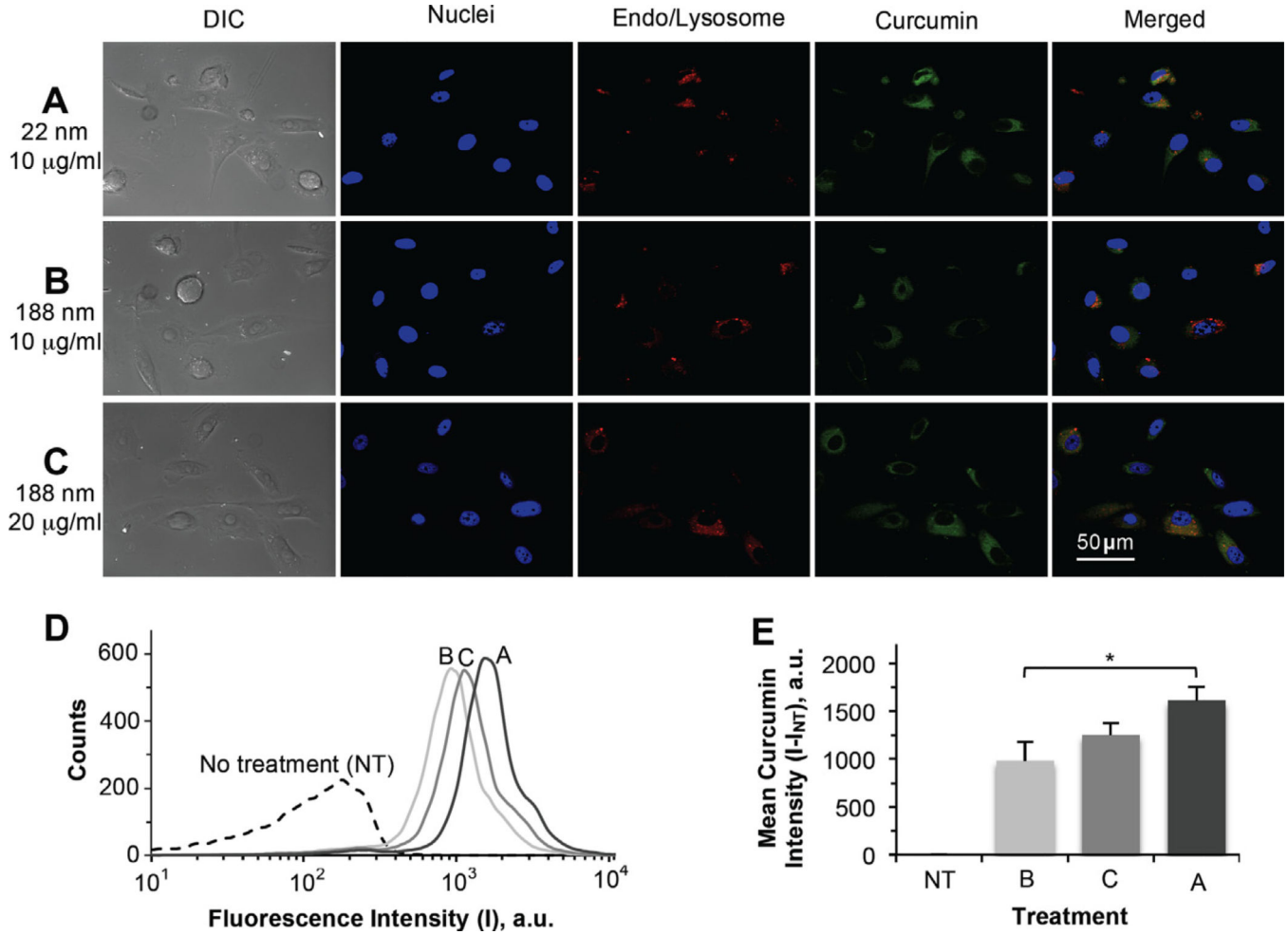

Fig. 3.

Effect of size (~22 vs. 188 nm) of the nCCM on its uptake by PC-3 cancer cells: (A–C) typical DIC and Apotome SIM fluorescence micrographs; (D) typical flow cytometry peaks of fluorescence intensity (*I*) in cells treated under the conditions for (A–C), together with that in NT control cells; and (**E**) a summary of the mean curcumin intensity ($I–I_{NT}$) in cells from flow cytometry of three independent runs, showing uptake of nCCM of either ~22 nm at 10 μg ml^{-1} or ~188 nm at 10 and 20 μg ml^{-1} in PC-3 cancer cells after 1 h incubation at 37 °C. The cells can take up the smaller (~22 nm) nCCM significantly faster. In (A–C), the blue and red stains are Hoechst and LysoTracker Red staining of cell nuclei and endo/lysosomes, respectively. The latter stains are spot-like under enlarged view. In (**E**), the mean curcumin intensity was calculated as the difference in fluorescence intensity in the cells with various treatment (*I*) and that with no treatment (I_{nt}) *p< 0.05.

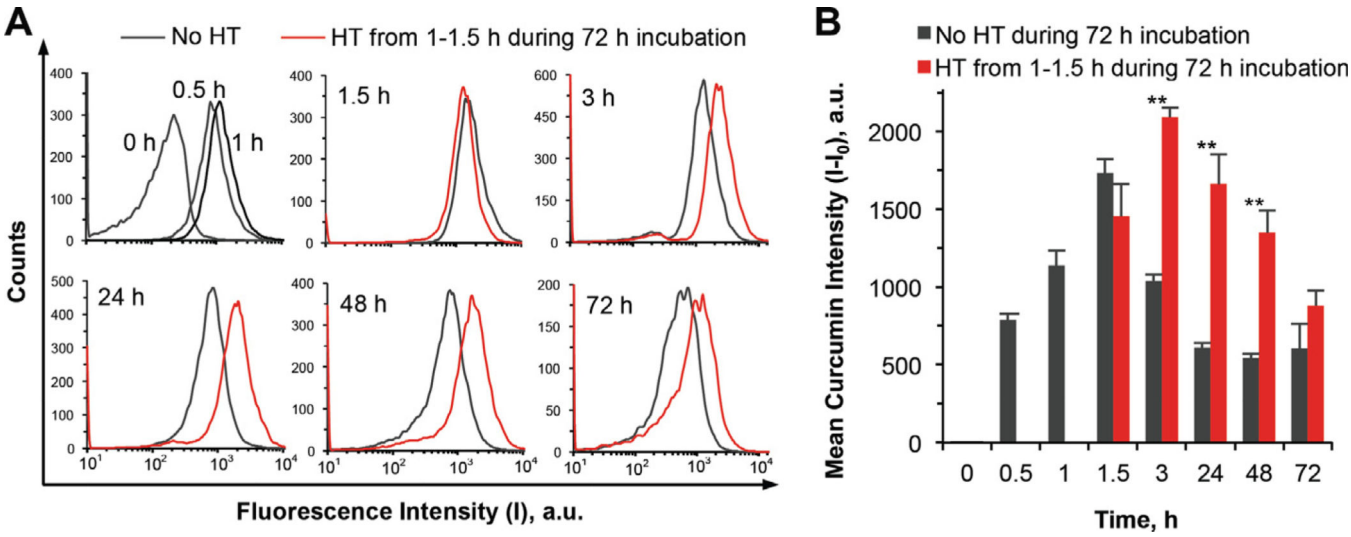

Fig. 4.

Effect of HT on cellular uptake of ~22 nm nCCM: (A) typical flow cytometry peaks of fluorescence intensity in PC-3 cancer cells and (B) mean curcumin intensity ($I - I_0$) in the cells at various times during incubation of the cells with the nCCM at 37 °C for 72 h either with or without a mild hyperthermia at 43 °C applied from 1 to 1.5 h: the HT treatment not only increases the peak uptake but also helps retain a much higher level of intracellular curcumin from 3 to 72 h. The mean curcumin intensity was calculated as the difference in fluorescence intensity in the cells at various time (I) and that at 0 h (I_0). **$p < 0.01$.

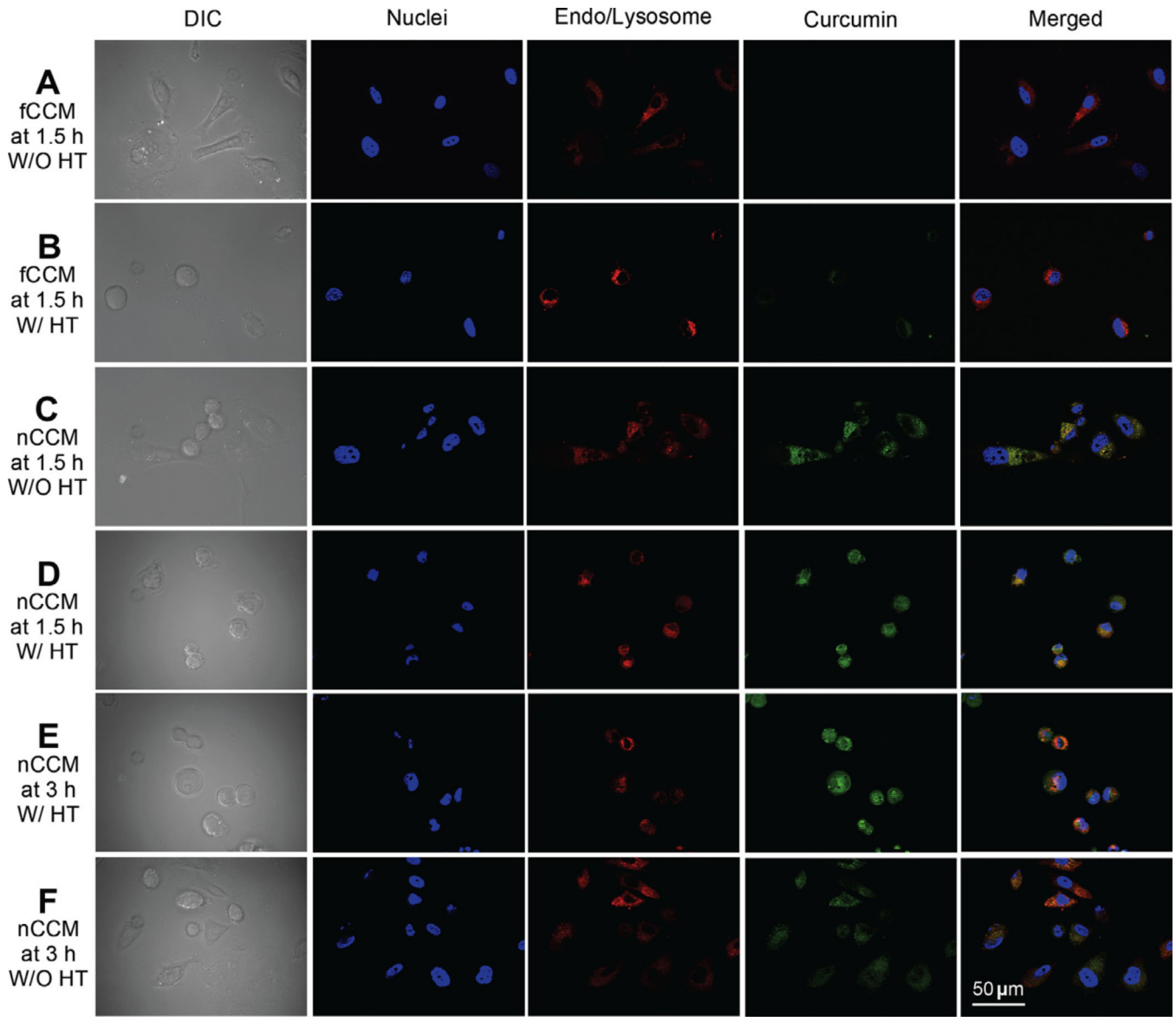

Fig. 5.

Effect of HT on cellular uptake and intracellular distribution of free and ~22 nm nCCM: typical DIC and Apotome SIM fluorescence micrographs of PC-3 cancer cells taken at 1.5 h (A–D) and 3 h (E and F) after incubating the cells with 10 μg ml^{-1} free curcumin (fCCM, A and B) or ~22 nm nCCM (C–F), either with or without HT applied from 1 to 1.5 h during the incubation. The blue and red stains are Hoechst and LysoTracker Red staining of cell nuclei and endo/lysosomes, respectively, and the latter stains are spot-like under enlarged view.

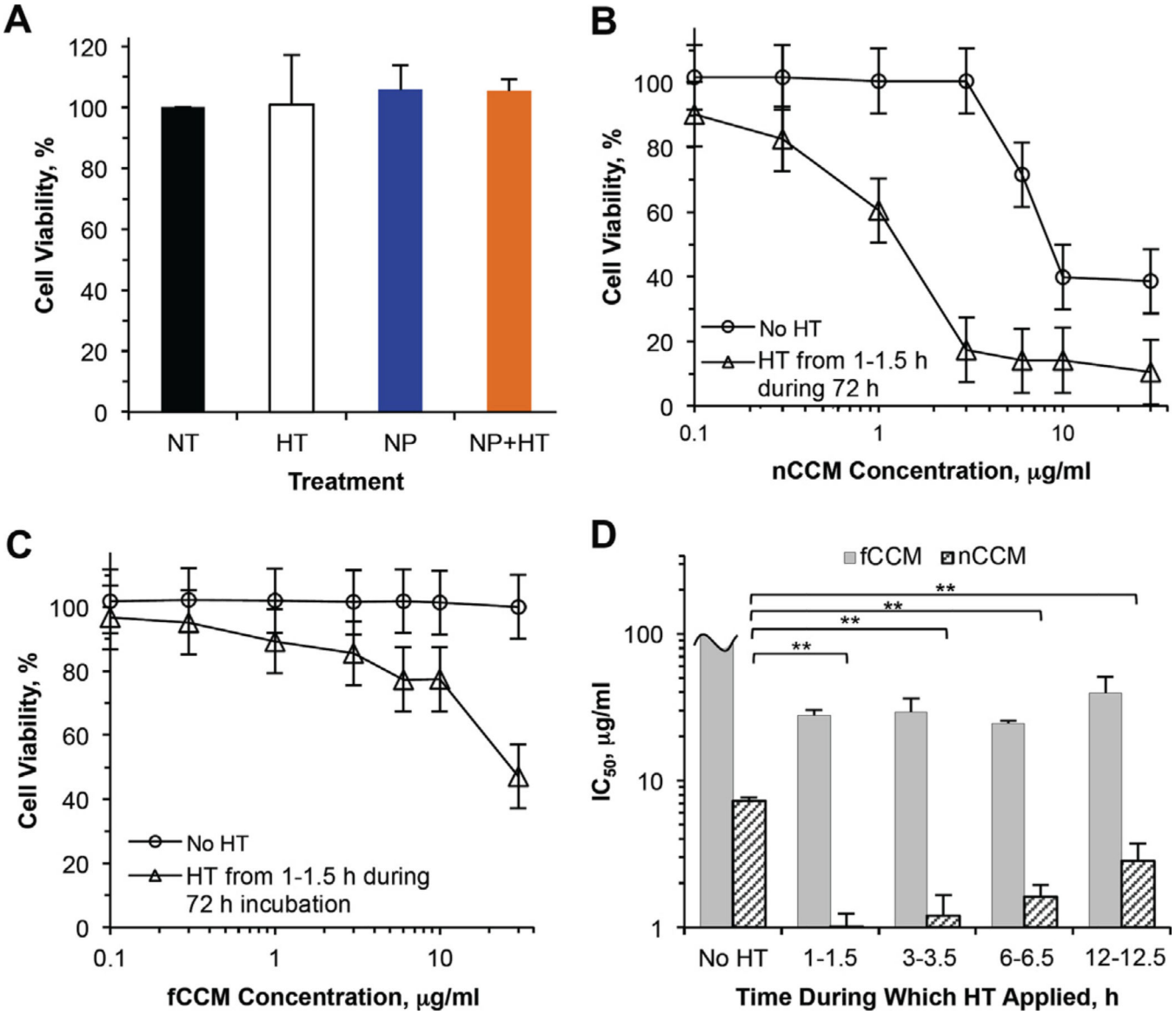

Fig. 6.

Toxicity to PC-3 cancer cells treated with HT, together with NP, fCCM, nCCM (~22 nm) and their combination with HT: (A) viability at day 3 of PC-3 cancer cells with NT, after treated with HT from 1 to 1.5 h alone, incubated with 1.845 mg ml^{-1} (corresponding to 30 μg ml^{-1} nCCM) NP for 3 days alone, and treated with the combination of the 3-day NP incubation and HT from 1 to 1.5 h during the incubation (NP + HT); viability of PC-3 cancer cells after 3-day incubation with ~22 nm nCCM (B) or fCCM (C) of various concentrations either without or with HT applied from 1 to 1.5 h during the incubation; and (D) IC_{50} (inhibitory concentration to reduce cell viability to 50%) determined using the data shown in (B) and (C) together with that shown in Fig. S5 for cells incubated for 3 days with fCCM and nCCM in combination with HT applied at 3–3.5 h, 6–6.5 h and 12–12.5 h: applying HT at 1–1.5 h during incubation with nCCM gives the best cancer cell destruction for the combined treatment on average, although the difference is statistically insignificant.

All treatments were done in culture medium containing 10% FBS. For unit conversion, 1 μg ml^{-1} is equivalent to 2.71 μM curcumin. All viability data were calculated with respect to control cells with no treatment. The IC_{50} data for fCCM with HT at 3–3.5, 6–6.5 and 12–12.5 h were obtained with slight linear extrapolation. $^{**}p < 0.01$.

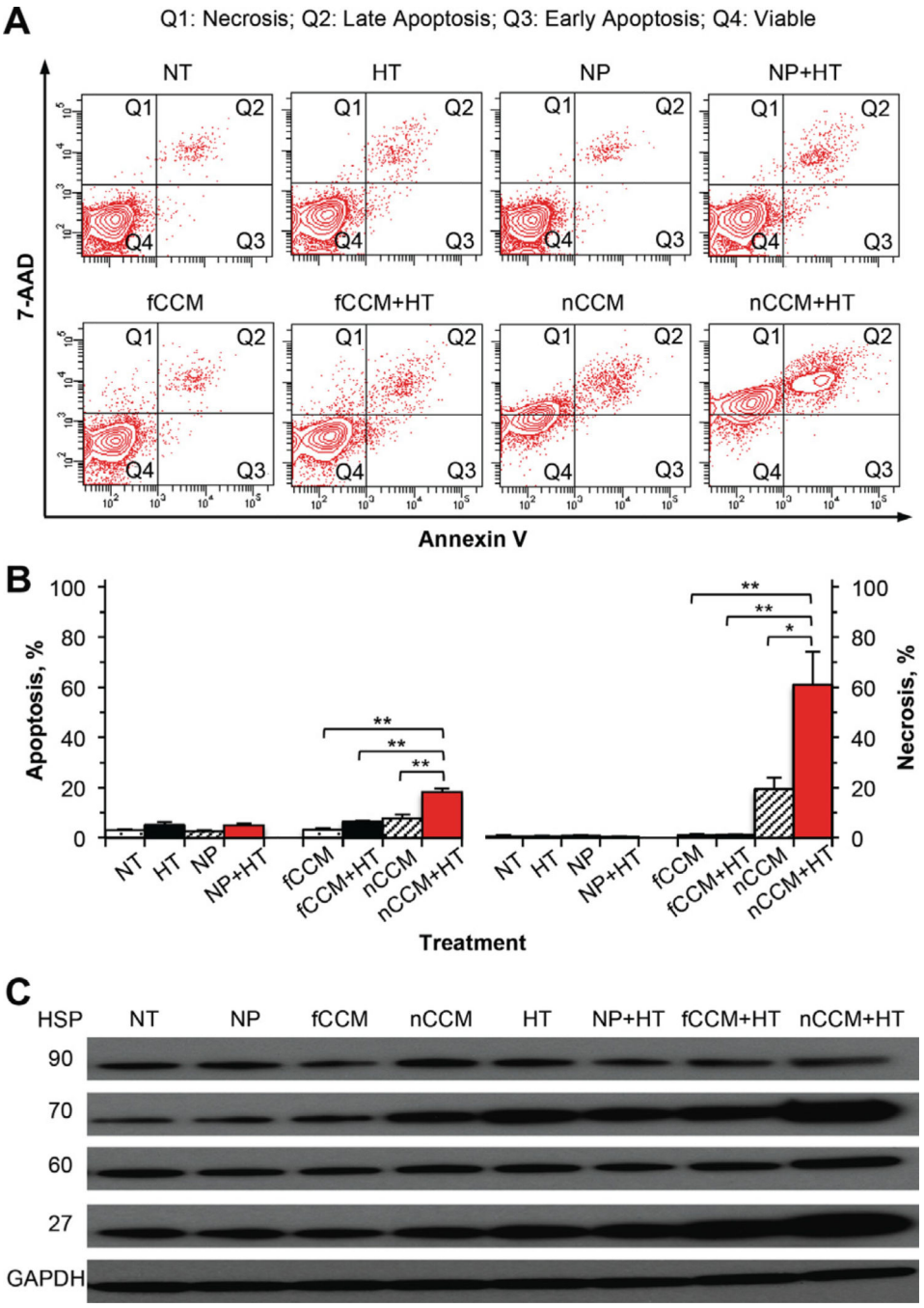

Fig. 7.

Mechanisms of injury to PC-3 cancer cells after incubated in medium for 2 days with NT, HT alone from 1 to 1.5 h during the incubation, NP alone, NP + HT, fCCM, fCCM + HT, nCCM (~22 nm) or nCCM + HT: (A) typical two-channel (for annexin V and 7-AAD) flow cytometry data showing the distribution of cells with necrosis in quadrant 1 (Q1), late apoptosis in Q2, early apoptosis in Q3 and viable cells in Q4; (B) a summary of the flow cytometry data from three independent runs; and (C) expression of four HSP showing

possible injury mechanism involving HSP 70 and 27 for the combined treatment of nCCM and HT. *$p < 0.05$; **$p < 0.01$.

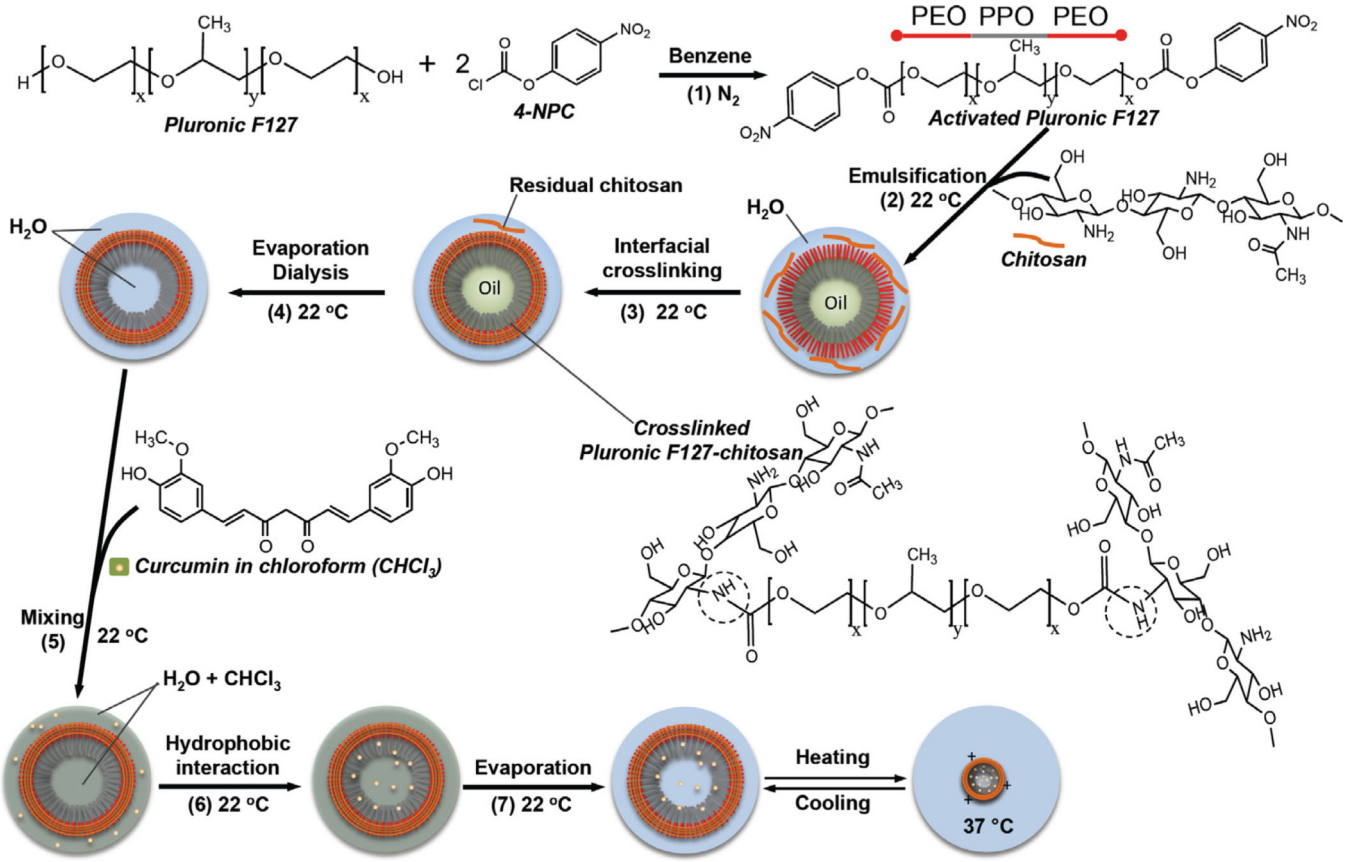

Scheme 1.

A schematic illustration of the chemistry and procedure for activating Pluronic F127, synthesizing Pluronic F127–chitosan NP and encapsulating free curcumin (fCCM) in the nanoparticle to obtain nanoparticle-encapsulated curcumin (nCCM): Pluronic F127 was activated (1) at both terminals using 4-NPC; nanoparticles were synthesized by oil-in-water emulsification (2), interfacial crosslinking with chitosan (3), and rotary evaporation and rigorous dialysis (4) to obtain aqueous solution of pure nanoparticles. Curcumin was encapsulated in the nanoparticle by mixing (under constant stirring) (5) solutions of free curcumin (fCCM) in chloroform ($CHCl_3$) and nanoparticles in water, utilizing (6) the high affinity between curcumin and the hydrophobic PPO core of the nanoparticles, and removing (7) chloroform by rotary evaporation. Also shown is an illustration of the thermal responsiveness of the resultant nCCM. The dashed circle in the formula of the crosslinked Pluronic F127–chitosan indicates the bonding between chitosan and Pluronic F127.

Table 1

EE and LC at different feeding ratios of fCCM to NP in weight together with diameter of the resultant nCCM determined by DLS.

Curcumin:NP ratio (w:w)	EE (%)	LC (%)	nCCM diameter, nm at 22 °C	nCCM diameter, nm at 37 °C
1:20	54.3 ± 0.1	3.4 ± 0.2	180.0 ± 6.6	188.1 ± 15.3
1:30	57.7 ± 15.6	2.4 ± 0.1	281.8 ± 25.2	289.4 ± 25.7
1:40	63.7 ± 2.0	2.2 ± 0.1	281.1 ± 23.0	21.1 ± 1.4
1:60	73.9 ± 4.5	1.6 ± 0.1	296.0 ± 15.3	22.0 ± 0.5
0	N/A	N/A	293.7 ± 33.1*	19.0 ± 1.3*

All data are presented as mean ± standard error of mean and N/A represents “not applicable”.

*Diameter of nanoparticles without any curcumin.